Global Sea Ice Extent – Level-3 product from EOS-06 (OCEANSAT-3)

Algorithm Theoretical Basis Document (ATBD)

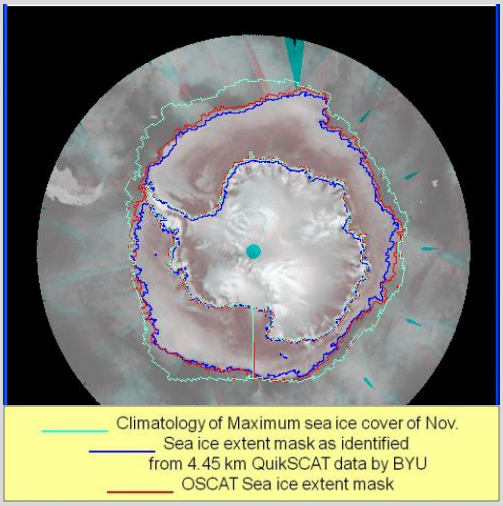

OSCAT derived Sea Ice Cover displayed over OSCAT backscatter data

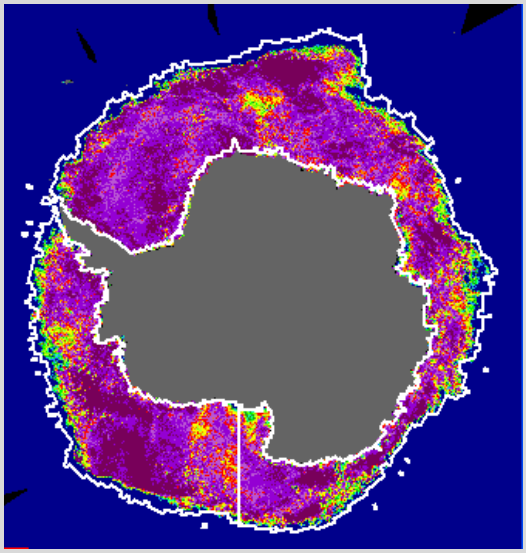

OSCAT Sea Ice Cover displayed over ASI sea ice concentration image

Cryosphere Sciences Division (CSD)
Geo-Sciences, Hydrology and Cryosphere Sciences and Applications Group (GHCAG)
Earth & Planetary Sciences and Applications Area (EPSA)
Space Applications Centre (SAC)

October 2021

DOCUMENT CONTROL AND DATA SHEET

1.	Date	October 2021
2.	Title	Global Sea Ice Extent – Level-3 product from EOS-06 (OCEANSAT-3)
3.	Doc. No.	SAC/EPSA/OCEANSAT-3/ATBD/OP-05/OCT-2021-V1
4.	Type of Report	Technical - Algorithm Theoretical Basis Document (ATBD)
5.	No. of Pages	10
6.	Authors	Purvee Joshi, Naveen Tripathi, Satyesh Kumar Ghetiya, Sushil Kumar Singh, Sandip R. Oza
7.	Originating Centre	Space Applications Centre (ISRO), Ahmedabad
8.	Abstract	In present study, an operational technique of generation of sea ice images and sea ice area (derived from the images) using level-4 data from Indian Scatterometer SCATSAT-1 has been discussed. A threshold-based technique developed based on hierarchical classification rules to generate super-resolution (2.25 km) daily sea ice images over the Antarctic for the years 2017 and 2018. The technique exploits 4 SCATSAT-1 data products, i.e. Gamma0 [Horizontal (H) and Vertical (V)] and Brightness Temperature (H and V) to classify sea ice, open water and other classes. Classification accuracy assessed by comparing SCATSAT-1 sea ice images with products obtained from AMSR2 sea ice concentration. The comparison shows that there is around 96.1% matching of sea ice classification between SCATSAT-1 and AMSR-2 sea ice concentration derived sea ice images. The observations from present work indicates that the super-resolution data of SCATSAT-1 is well capable of distinguishing sea ice from water.
9.	Keywords	Oceansat-3, Sea ice extent, Gamma nought, Brightness Temperature, Scatterometer
10.	Approving Authority	Oceansat-3 ATBD Review Committee
11.	Classification	Unrestricted
12.	Circulation	Open

Algorithm theoretical basis document (ATBD) for Global Sea Ice Extent from EOS-6 (OCEANSAT-3)

1.0 Algorithm Specifications:

Version	Date	Prepared by	Description
1.0	October 2021	Purvee Joshi, Naveen Tripathi, Satyesh Kumar Ghetiya, Sushil Kumar Singh, Sandip R. Oza	Global Sea Ice Extent – Level-3 product from EOS-06 (OCEANSAT-3)

2.0 Introduction

Sea ice has an intense impact on the polar environment, ocean circulation, weather and regional climate. Unexpected melting of sea ice, which is considered as one of the climate change effects, has become a potential threat to the Earth's climate. The regular monitoring of sea ice and its extent has become very important towards understanding of sea ice temporal dynamics. In this study, we present an operational technique of generation of sea ice images and sea ice area (derived from the images) using level-4 data from Indian Scatterometer SCATSAT-1. Using hierarchical classification rules, the threshold-based technique has been developed and applied to generate super-resolution (2.25 km) daily sea ice images over the Antarctic for the years 2017 and 2018. The technique uses four SCATSAT-1 data products, i.e. Gamma0 [Horizontal (H) and Vertical (V)] and Brightness Temperature (H and V) to classify sea ice, open water and other classes. Classification accuracy has been assessed by comparing SCATSAT-1 sea ice images with those obtained from AMSR2 sea ice concentration data. The comparison shows that there is around 96.1% matching of sea ice classification between SCATSAT-1 and AMSR-2 SIC derived sea ice images. Hence, it indicates that the super-resolution data of SCATSAT-1 is well capable of distinguishing sea ice from water.

3.0 Background: Sea Ice Extent - Polar - Arctic & Antarctic using Scatterometers

SCATSAT-1 is a continuity mission to Indian satellite OceanSat-2, and launched by the Indian Space Research Organization (ISRO) in the year of 2016. It orbits at an altitude of 723 km. It provides data in the range of Ku-band (operating at 13.515 GHz). The inner and outer beams of Scatsat-1 are configured in horizontal and vertical polarization respectively for both transmit and receive modes with a revisit time of 2 days and an approximate swath of 1400-1800 km. Though, the primary function of the

sensor is to generate wind vector at either 50×50 km or 25×25 km, but its data is also found to be useful in polar sea-ice studies, along with many other studies.

In the current study, Level - 4 data products have been used which has spatial resolution as high as 2.25 km (operational version 1.1). The Level 4 products are generated from Level 1B products. These high-resolution products are generated using Scatterometer Image Reconstruction (or SIR) technique (Long et al., 1993). The products are generated in six bands namely sigma-0 (σ0), gamma-0 (Ɣ0) and brightness temperature (Tb) in both horizontal and vertical polarization (more details about the product in the manual of SCATSAT1 DP Team, 2017). Depending on combinations of polarization/pass/look and temporal extent of data, various sub-categories of Level 4 products are defined (more details about the product in the manual of SCATSAT1 DP Team, 2017). The dataset used in this study is the NorthPolar24 and SouthPolar24 which are archived at the ISRO's data archival website, Meteorological & Oceanographic Satellite Data Archival Centre, MOSDAC (https://mosdac.gov.in/). We have used Tb in both horizontal and vertical polarization namely BH and BV respectively and similarly Ɣ0 in both horizontal and vertical polarization namely GH and GV respectively.

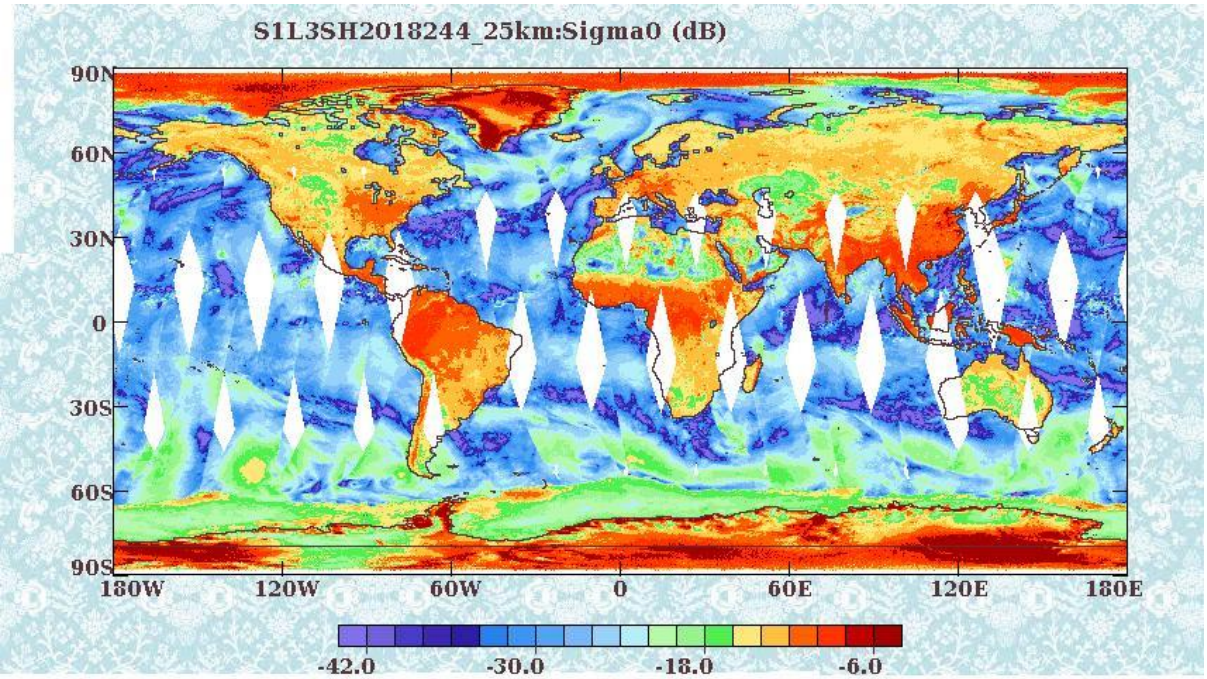

Figure 1: *The coverage of SCATSAT-1 represented with Sigma0 (dB) data for 1st of September, 2018*

For statistical comparison and accuracy assessment, Sea Ice Concentration (SIC) produced using Advanced Microwave Scanning Radiometer 2 (AMSR2) (further

referred as SIC image) was used as the reference images for error analysis. AMSR2 sensor on-board satellite Global Change Observation Mission-Water (GCOM-W) of Japan Aerospace Exploration Agency (JAXA) have been used for daily data over sea ice region of the Earth with spatial resolution of 3.125 km. With reference to ARTIST (Arctic Radiation and Turbulence Interaction STudy), the ARTIST Sea Ice (ASI) algorithm was developed which has been used to generate the data (Spreen et al., 2008). National Snow and Data Ice Centre (NSIDC) provides the continuous series of dataset of daily sea ice concentration over sea ice region of the Earth. More details of satellites data are given in Table 1.

Table No. 1: *Specifications of the satellite data which are used in this study*

Source of Data	Special Resolution (km)	Temporal Resolution	Data Type	Version	Frequency
SCATSAT-1	2.25	Daily	Sea ice extent	1.3	13.515 GHz
AMSR2	3.125	Daily	Sea ice concentration	5.4	89 GHz

4.0 Methodology

The identification of sea-ice has frequently been reported as one of the most important task for deriving the sea-ice parameters and to avoid erroneous retrieval of wind vector over sea-ice infested oceans using space-borne scatterometer data. Discrimination between sea-ice and ocean is ambiguous under the high wind and/or thin/scattered ice conditions. An algorithm and software has been developed and evaluated at SAC (ISRO) and made operational in Oceansat-2 OSCAT and SCATSAT-1 Data Product chain.

The similar software module with minor revision will be followed for the generation of sea ice flag in EOS-6 (Oceansat-3) scatterometer data product generation. The sea ice flag image is being updated for every orbit in the DP chain and latest image at 00 Hrs is considered as daily image for the day of concern. This image will further be used for the final global sea ice product.

3.1 Physics of the problem:

Ocean backscatter varies considerably as a function of the wind speed and wind direction relative to the radar look-angle. It also varies over different sea-ice types at

different seasons (Ulaby et al., 1986). At low wind speeds, the average backscatter from the ocean is generally lower than that from ice. Ice and ocean may exhibit similar mean backscatter at higher wind speeds. During summer melts, ice backscatter drops generally by 5 dB and therefore, the ice-ocean backscatter contrast diminishes (Haarpaintner et al., 2004). Oza et al. (2011) have developed a spatio-temporal coherence based sea-ice identification procedure (Oza et al. 2011). The algorithm has been implemented in the generation of sea ice flag in OSCAT data products. The major points of the algorithm have been summarized as discussed below.

3.2 Spatio-temporal coherence properties of sea ice:

Haarpaintner et al (2004) have used previous one day status as the first approximation to account for ocean noise. However, longer periods of strong winds can still prevail as ocean noise during different seasons. The wind fields, generally, exhibit variability over a time scale of a few hours to a few days. The sea-ice cover exhibits variability over a time scale of a few weeks to a few months. In general, the time scales of the two processes are different. This suggests that both can be distinguished better in time domain. Therefore, the data acquired over a few consecutive days was utilized to resolve the ambiguity. Since, wind fields are most likely to vary significantly over 3-4 days, it is appropriate to use the data of previous 4 days to remove the sea-ice identification ambiguity.

During the growth/melt of the sea-ice, it grows/melts around the previously existing ice, and hence follows spatial coherence. This property of sea-ice growth was utilized by applying the 3 x 3 pixel moving window filter to make use of the spatial coherence pattern. This will reduce the random appearance of ocean/sea-ice pixels. The spatio-temporal coherence largely reduces the identification inaccuracies in both the hemispheres.

3.3 Algorithm description:

The flow diagram of the steps followed for the sea-ice identification is shown in Figure 1. The daily backscatter images (H & V) the previous four days were utilized to check the spatio-temporal coherence. Non-polar area was masked using the climatological maximum sea ice extent for the month, in which majority of the four input image falls.

The hierarchical classification rules applied to identify the sea-ice and ocean classes are given below,

i. σ0H > -25 dB in winter and > -28 dB in summer

ii. σ0V > -25 dB in winter and > -28 dB in summer

iii. APR < APR0 for winter and summer; APR0=Derived optimum APR threshold

iv. 4-Day Standard deviation (SD0) < 4 dB in winter and < 5 dB in summer; where SD0 is the SD of σ0H or σ0V, whichever is higher

v. Condition for temporal coherence: Conditions (i) to (iv) should be satisfied at least for the median number of images (in present case 3 out of four images).

vi. Condition for spatial coherence: Median number of pixels, or more, in the moving window should be sea-ice (i.e. 5 or more in a 3x3 window)

Here, the rules (i), (ii) and (iv) for the σ0H, σ0V and Standard Deviation (SD) were taken from Haarpaintner et al (2004), rule (iii) is a modified version with an optimized APR **threshold,** and rules (v) and (vi) were devised by the authors to improve the classification accuracy based on the time-scales of wind field and sea ice evolution processes.

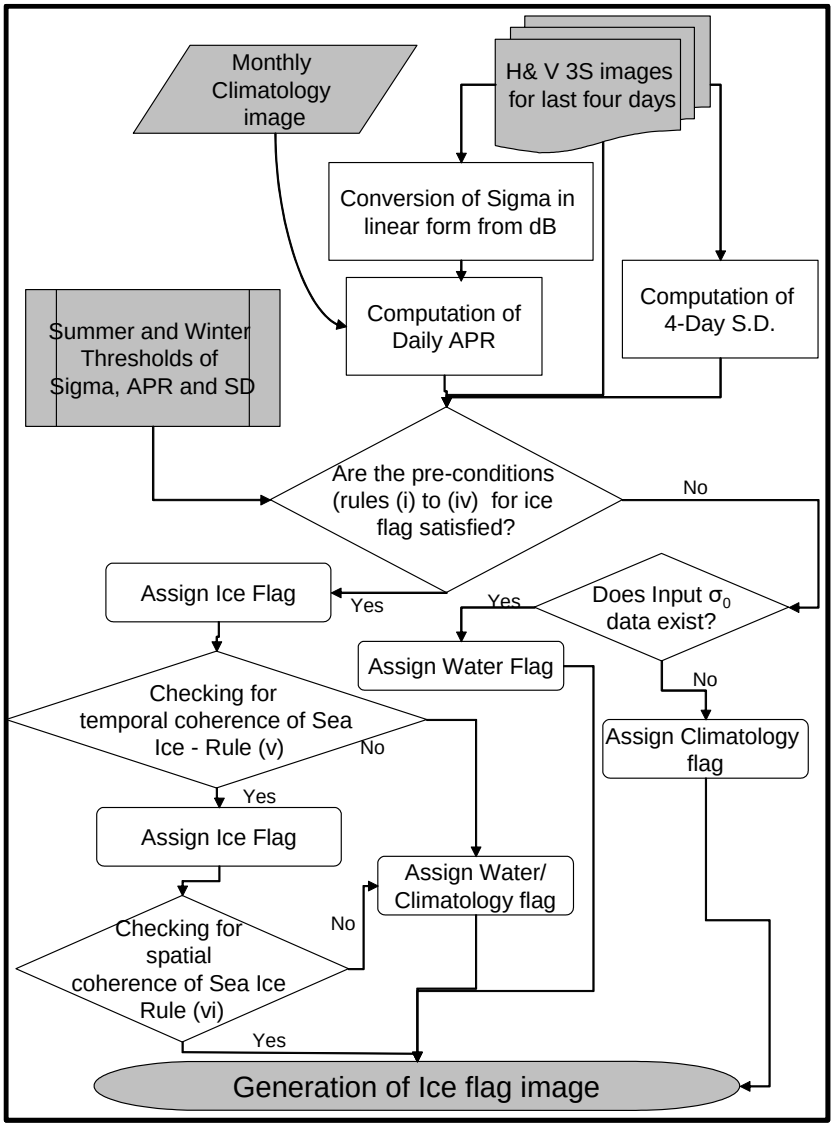

Figure 1: *Flow diagram showing steps followed for se ice identification*

Following codes (Table 2) are being assign for various surface type in the final product.

Table 2: *Codes for different surface types*

Value	Feature
0	Open Ocean
2	LandIce-Ocean mixed
3	Land
10	Open Ocean in polar region
11	Sea Ice
111	Data Problem

4.0 Error Analysis and Accuracy Assessment

Sample image of 21st February 2021, obtained from the MOSDAC is as given below.

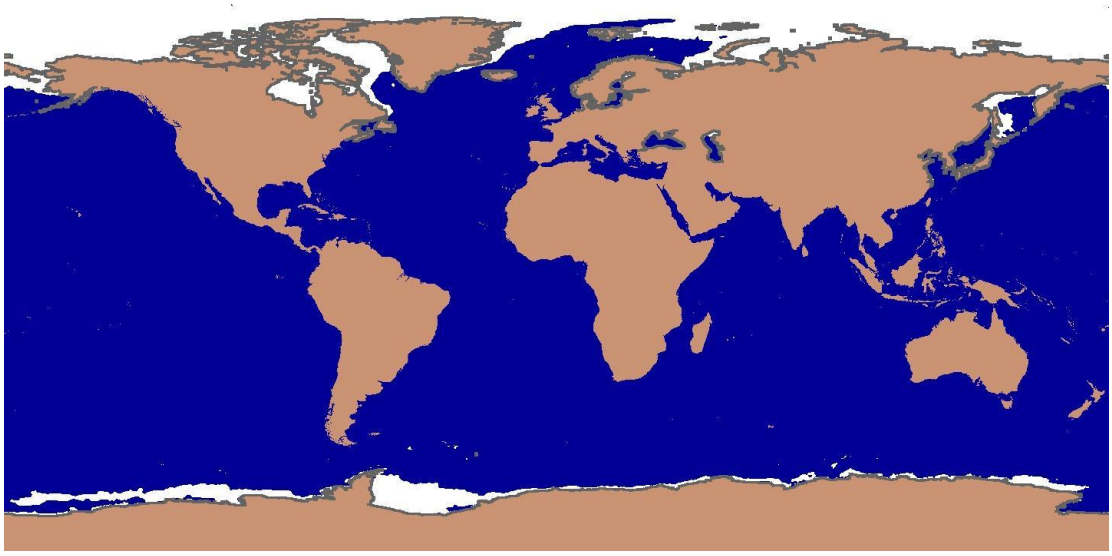

An evaluation of OSCAT derived sea ice flags has been carried out using (i) QUISCKSCAT derived ice extent obtained from BYU site and (ii) passive microwave radiometer derived sea ice cover obtained from ASI site. The comparison is as shown in figure 2.

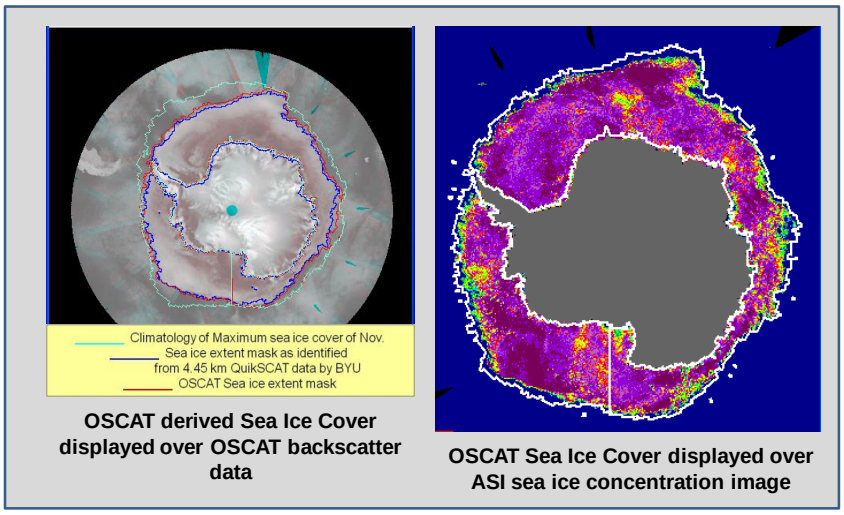

Figure 2: *Comparison between i) QUISCKSCAT derived ice extent obtained from BYU site and (ii) passive microwave radiometer derived sea ice cover obtained from ASI site.*

The comparison with ASI data derived from passive microwave radiometer is slightly under estimates the sea ice, which could be due to the sensitivity of scatterometer towards the presence of sea ice is higher compared to radiometer. It is observed that OSCAT derived sea ice cover closely follows the QuikSCAT derived ice cover obtained from BYU.

The additional module developed for SCATSAT is expected to improve the identification procedure. This module utilizes the spatio-temporal coherence based 3S sea ice flag code image as a-priori information and further improves the identification by considering the real-time slice/composite level Sigma-0 and BT values.

6.0 Future scope

There is need for long term monitoring of sea ice extent over polar sea ice for statistically significant conclusion addressing the mass balance scenarios of Polar Regions. The sea ice extent observation from Oceansat-3 data along with continuity from previous scatterometers can provide evidences regarding the impact of climate change in most sensitive polar region. There will be a scope to refine the detection algorithm based on adaptive threshold method using brightness temperature data from Oceansat-3.

7.0 Acknowledgments

The authors would like to sincerely thank GD, GHCAG, PD & APD Oceansat-3 for their valuable guidance and suggestions.

8.0 References:

1. Agnew, T., & Howell, S. (2003). The use of operational ice charts for evaluating passive microwave ice concentration data. Atmosphere-ocean, 41(4), 317-331.
2. Al-amri, S. S., Kalyankar, N. V., & Khamitkar S.D. (2010). Image segmentation by using threshold Techniques. Journal of Computing, Volume 2, Issue 5, May, 2010, ISSN 2151-9617
3. Cavalieri, D. J., Gloersen, P., & Campbell, W. J. (1984). Determination of sea ice parameters with the Nimbus 7 SMMR. Journal of Geophysical Research: Atmospheres, 89(D4), 5355-5369.
4. Cavalieri, D. J., Gloersen, P., Parkinson, C. L., Comiso, J. C., & Zwally, H. J. (1997). Observed hemispheric asymmetry in global sea ice changes. Science, 278(5340), 1104-1106.
5. Cavalieri, D. J., Parkinson, C. L., Gloersen, P., Comiso, J. C., & Zwally, H. J. (1999). Deriving long-term time series of sea ice cover from satellite passive-microwave multisensor data sets. *Journal of Geophysical Research: Oceans*, *104*(C7), 15803-15814.
6. Cho, K., & Naoki, K. (2015). Advantages of AMSR2 for Monitoring Sea Ice from Space. In *Proc. of Asian Conference on Remote Sensing, Manila, Philippines, Oct* (pp. 19-23).
7. Comiso, J. C. (1995). *SSM/I sea ice concentrations using the bootstrap algorithm* (Vol. 1380). National Aeronautics and Space Administration, Goddard Space Flight Center.
8. Comiso, J. C., Cavalieri, D. J., Parkinson, C. L., & Gloersen, P. (1997). Passive microwave algorithms for sea ice concentration: A comparison of two techniques. Remote sensing of Environment, 60(3), 357-384.
9. Congalton, R. G. (1991). A review of assessing the accuracy of classifications of remotely sensed data. *Remote sensing of environment*, *37*(1), 35-46.
10. Drue, C., & Heinemann, G. (2004). High-resolution maps of the sea-ice concentration from MODIS satellite data. *Geophysical research letters*, *31*(20).
11. Gignac, C., Bernier, M., Chokmani, K., & Poulin, J. (2017). IceMap250—Automatic 250 m sea ice extent mapping using MODIS data. *Remote Sensing*, *9*(1), 70.
12. Haarpaintner, J., Tonboe R. T., and Long, D. G., 2004. Automatic Detection and Validity of the Sea-Ice Edge: An application of Enhanced-Resolution QuikSCAT/ Sea Winds Data. IEEE Trans. Geosci. and Rem. Sensing, 42:1433-1443.
13. Hall, D. K., Key, J. R., Casey, K. A., Riggs, G. A., & Cavalieri, D. J. (2004). Sea ice surface temperature product from MODIS. *IEEE transactions on geoscience and remote sensing*, *42*(5), 1076-1087.
14. Ivanova, N., Johannessen, O. M., Pedersen, L. T., & Tonboe, R. T. (2014). Retrieval of Arctic sea ice parameters by satellite passive microwave sensors: A comparison of eleven sea ice concentration algorithms. *IEEE Transactions on Geoscience and Remote Sensing*, *52*(11), 7233-7246.

15. Ivanova, N., Pedersen, L. T., Tonboe, R. T., Kern, S., Heygster, G., Lavergne, T., & Shokr, M. (2015). Inter-comparison and evaluation of sea ice algorithms: towards further identification of challenges and optimal approach using passive microwave observations. *The Cryosphere*, *9*(5), 1797-1817.
16. Kaleschke, L., & Kern, S. (2002). ERS-2 SAR image analysis for sea ice classification in the marginal ice zone. In *IEEE International Geoscience and Remote Sensing Symposium* (Vol. 5, pp. 3038-3040). IEEE.
17. Kaleschke, L., Lüpkes, C., Vihma, T., Haarpaintner, J., Bochert, A., Hartmann, J., & Heygster, G. (2001). SSM/I sea ice remote sensing for mesoscale ocean-atmosphere interaction analysis. Canadian Journal of Remote Sensing, 27(5), 526-537.
18. Kern, S., & Heygster, G. (2001). Sea-ice concentration retrieval in the Antarctic based on the SSM/I 85.5 GHz polarization. *Annals of Glaciology*, *33*, 109-114.
19. Lubin, D., Garrity, C., Ramseier, R., & Whritner, R. H. (1997). Total sea ice concentration retrieval from the SSM/I 85.5 GHz channels during the Arctic summer. Remote sensing of environment, 62(1), 63-76.
20. Meier, W. N., & Stewart, J. S. (2019). Assessing uncertainties in sea ice extent climate indicators. *Environmental Research Letters*, *14*(3), 035005.
21. Meier, W. N., Gallaher, D., & Campbell, G. G. (2013). New estimates of Arctic and Antarctic sea ice extent during September 1964 from recovered Nimbus I satellite imagery. Cryosphere, 7(2).
22. Oza, S. R., Singh, R. K. K., Vyas, N. K., Gohil, B. S. and Sarkar, Abhijit, 2011. Spatio-temporal coherence based technique for near-real time sea-ice identification from scatterometer data. Journal of Indian Society of Remote Sensing, 39:147-152.
23. Parkinson, C. L. (2000). Variability of Arctic sea ice: The view from space, an 18-year record. Arctic, 341-358.
24. Parkinson, C. L., & Cavalieri, D. J. (2002). A 21 year record of Arctic sea-ice extents and their regional, seasonal and monthly variability and trends. *Annals of Glaciology*, *34*, 441-446.
25. Parkinson, C. L., Cavalieri, D. J., Gloersen, P., Zwally, H. J., & Comiso, J. C. (1999). Arctic sea ice extents, areas, and trends, 1978–1996. *Journal of Geophysical Research: Oceans*, *104*(C9), 20837-20856.
26. Scatsat1 DP Team, (2017). SCATSAT-1 Level 4 Data Products Format Document Microwave Data Processing Division Signal and Image Processing Group Space Applications Centre Ahmedabad. SC1/DP/L4FORMAT-DOC/V1.1/JUL2017
27. Soh, L. K., Tsatsoulis, C., Gineris, D., & Bertoia, C. (2004). ARKTOS: An intelligent system for SAR sea ice image classification. *IEEE Transactions on Geoscience and Remote Sensing*, *42*(1), 229-248.
28. Spreen, G., Kaleschke, L., & Heygster, G. (2008). Sea ice remote sensing using AMSR-E 89-GHz channels. *Journal of Geophysical Research: Oceans*, *113*(C2).

29. Srigyan M., Basu A., Mukherjee A., Sengupta P. & Sen. J. (2017). Identification of paleochannels in and around Chandraketugarh, Ganges Delta through remote sensing techniques using fuzzy inference system Archaeological and Anthropological Scienceshttps://doi.org/10.1007/s12520-017-0577-3
30. Svendsen, E., Matzler, C., & Grenfell, T. C. (1987). A model for retrieving total sea ice concentration from a spaceborne dual-polarized passive microwave instrument operating near 90 GHz. International Journal of Remote Sensing, 8(10), 1479-1487.
31. Swan, A. M., & Long, D. G. (2012). Multiyear Arctic sea ice classification using QuikSCAT. *IEEE transactions on geoscience and remote sensing*, *50*(9), 3317-3326.
32. Swift, C. T., & Cavalieri, D. J. (1985). Passive microwave remote sensing for sea ice research. *Eos, Transactions American Geophysical Union*, *66*(49), 1210-1212.
33. Ulaby, F.T., Moore, R. K., and Fung, A. K., 1986. Radar measurements of sea-ice, in Microwave Remote Sensing, Vol. 3, Artech House, Norwood, 1986. Chap. 20-4.
34. Upadhyay, K., Tripathi, N., Vachharajani, B., Rajak, D.R. and Bahuguna, I.M., 2021. Deriving Sea Ice Images from Super Resolution SCATSAT-1 Data over the Antarctic: Operational Method and Accuracy Assessment. *Journal of the Indian Society of Remote Sensing*, pp.1-7.
35. Walsh, J. E. (1983). The role of sea ice in climatic variability: Theories and evidence. *Atmosphere-Ocean*, *21*(3), 229-242.
36. Yu, Q., & Clausi, D. A. (2007). SAR sea-ice image analysis based on iterative region growing using semantics. *IEEE Transactions on Geoscience and Remote Sensing*, *45*(12), 3919-3931.